
PERGAMON

Journal of the Mechanics and Physics of Solids
49 (2001) 2015–2030

JOURNAL OF THE
MECHANICS AND
PHYSICS OF SOLIDS

www.elsevier.com/locate/jmps

The effect of hole size upon the strength of metallic and polymeric foams

N.A. Fleck *, O.B. Olurin, C. Chen, M.F. Ashby

Engineering Department, Cambridge University, Trumpington Street, Cambridge CB2 1PZ, UK

Abstract

Tensile and compressive tests have been performed on centre-hole panels, made from three types of metallic foams and two polymeric foams. In compression, the foams fail in a ductile, notch-insensitive manner, in support of a "net section strength" criterion. In tension, a ductile–brittle transition is observed for some of the foams at sufficiently large specimen sizes: for a small hole diameter the net section strength criterion is obeyed, whereas for a large hole a local stress criterion applies and the net section strength is reduced. For a number of the foams, the panel size was not sufficiently large to observe this ductile–brittle switch in behaviour. The predictions of a cohesive zone model are compared with the measured strengths and are found to be in good agreement.

Keywords: Foams; Monotonic and fatigue properties; Notch sensitivity; Cohesive zone model; Transition flaw size

1. Introduction

Metallic foams have potential for use in the cores of sandwich panels, shells and tubes, for use as ultra-light materials for air, sea and ground-based vehicles, for application to heat dissipation, and for energy absorption (Gibson and Ashby, 1997; Ashby et al. 2000; Lu et al. 1998; Evans et al. 1999). Polymeric foams are excellent energy absorbers and have already found a wide range of applications in the automobile and packaging industry (Gibson and Ashby, 1997).

Recent developments in manufacturing techniques have made metallic foams commercially viable, and the foaming of a wide range of metals is now a practical possibility. Metallic foam manufacturing techniques include solid state powder methods,

* Corresponding author. Tel.: +44-1223-332-650; fax: +44-1223-332-662.
E-mail address: nafl@eng.cam.ac.uk (N.A. Fleck).

0022-5096/01/$ - see front matter
PII: S0022-5096(01)00033-3

gas-blowing processes, liquid state processing, casting with a blowing agent and metal deposition onto a polymer "precursor" (Ashby et al. 2000). Polymeric foams are usually made by introducing gas bubbles into hot liquid polymer (Gibson and Ashby, 1997). The successful application of foams depends not only upon inventing new techniques to produce foams which are cheap and of improved quality, but also upon the development of a detailed understanding of their mechanical properties. Studies have shown that foams behave differently in tension and compression. In compression, they display three successive regimes of behaviour: linear elastic, deformation at a constant plateau stress σ_{pl} and then a final steepening stress–strain response associated with the contact of opposing cell walls at nominal compressive strains of 50–90%. In tension, the initial elastic regime is followed by yield, and then the initiation and propagation of a dominant tensile crack at a macroscopic tensile strain in the range 1–10%, depending upon the properties of the cell wall material (Olurin et al. 2000).

The failure of engineering structures frequently originates at stress concentrations caused by macroscopic geometric discontinuities such as holes, grooves and shoulders. Since holes are likely to be cut in foams for fastening, cooling and other purposes, their effect upon strength is of practical concern. It is recalled that fully dense metals containing a hole can fail either by net section yielding or by a local maximum stress criterion depending upon the hole diameter relative to an intrinsic material length scale, termed here the *transition hole diameter* D_t. These concepts have been discussed by Suo et al. (1993), Bao and Suo (1992), and Cox and Marshall (1994) for the case of composites materials, and by Fleck et al. (1994) for both monotonic and cyclic loading of engineering materials. The aim of the current study is to investigate the effect of a centre-hole upon the tensile and compressive strengths of metallic and polymeric foams.

2. Material specification and experimental procedure

2.1. Materials

Three types of metallic foam (*Alporas*[1], *Alcan*[2] and *Inco*[3] foams) and two polymeric foams (a ductile *Divinycell*[4] PVC foam and a brittle Polystyrene foam[5]) are investigated. Alporas foam, of relative density $\bar{\rho}=11\%$, is a closed cell aluminium alloy foam of composition Al–Ca 5–Ti 3 (wt%). Alcan foam of relative density $\bar{\rho}=5.6\%$ is a closed cell foam made from the cast aluminium alloy A356—Al–Si 7–Mg 0.3 (wt%), with SiC particles. Alcan foam is made in the liquid state by blowing with air or nitrogen, whereas Alporas is produced by stirring a blowing agent (titanium hydride)

[1] Supplier: Shinko Wire Company Ltd., 10-1, Nakahama-machi, Amagasaki-shi, 660 Japan.

[2] Supplier: Alcan International Ltd., Box 8400, Kingston, Ontario, K7L 5L9, Canada.

[3] Supplier: Inco Limited, Research Laboratory, Sheridan Park, Mississauga, Ontario L5K 1Z9, Canada.

[4] Supplier: Divinycell International Limited, Gloucester GL4 3SJ, U.K.

[5] Supplier: Vencel Resil Ltd., Arndale House, 18-20 Spiral Str., Dartford, Kent, DA1 2HT.

Table 1
Material parameters for the foams

	E^a (GPa)	ν^b	$\varepsilon_y{}^a$ (%)	$\sigma_y{}^a$ (MPa)	σ_{UTS} (MPa)	N^a	α^c	J_{IC} (kJ m^{-2})	$\delta_0{}^d$ (mm)	$D_t{}^e$ (mm)	ℓ (mm)
Alporas	0.34	0.2	0.45	1.53	1.81	0.15	1.8	1.55	1.71	53.2	3.5
Alcan	0.21	0.2	0.467	0.98	1.14	0.07	2	0.286	0.5	15.3	11.5
Inco	0.271	0.2	0.299	0.81	1.15	0.13	2	1.19	2.08	81.0	0.5
Alulight	2.16	0.2	0.185	4.0	6.00	0.20	2	2.15	0.841	42.8	1.00
Divinycell	0.18	0.2	2.93	5.28	6.60	0.13	2	1.00	0.303	1.41	0.25
Polystyrene	0.01	0.2	0.08	0.08	0.28	0.71	2	0.418	3.00	17.7	0.045

[a]See Eq. (7) for definition.
[b]Assumed Poisson's ratio.
[c]See Eq. (3) for definition.
[d]$\delta_0 = 2J_{IC}/\sigma_{UTS}$.
[e]$D_t = EJ_{IC}/\pi(1-\nu^2)\sigma_{UTS}^2$.

Table 2
The specimen geometry and dimensions for the uniaxial tension and compression tests of unnotched foams

	Geometry	L (mm)	W (mm)	B (mm)
Alporas (tension & compression)	Cuboid	70	70	25
Alcan (tension & compression)	Cuboid	115	115	70
Inco (tension)	Dogbone	30	20	1.4
Divinycell (tension)	Dogbone	50	75	10
Divinycell (compression)	Cuboid	50	75	50
Polystyrene (tension)	Dogbone	45	30	7
Polystyrene (compression)	Cuboid	45	30	7

within the melt. Inco nickel foam, of relative density $\bar{\rho} = 4.3\%$, is an open cell foam manufactured by vapour phase deposition onto a polymeric foam precursor which is later burned out; the hollow cell edges are made up of fine grained, polycrystalline nickel (Kriszt and Ashby, 1997). Divinycell PVC foam (grade H200, $\bar{\rho} = 14.3\%$) is manufactured by introducing gas bubbles into the hot polymeric melt, whereas the Polystyrene foam ($\bar{\rho} = 3.0\%$) is produced by the chemical release of a gassing agent within the melt. Details of the composition are documented elsewhere for Alporas foam (Olurin et al. 2000), Alcan foam (Olurin et al. 2000), Inco foam (Kriszt and Ashby, 1997) and Divinycell foam (Divinycell Technical Manual, 1995) and their main mechanical properties are summarised in Table 1, with definition of the material parameters listed in the table.

2.2. Uniaxial tension and compression tests on foams

First, the uniaxial behaviours of unnotched foams were measured using cuboid specimens in compression, and either cuboid or dogbone specimens in tension. A summary of the specimen dimensions is given in Table 2, with L denoting the specimen length,

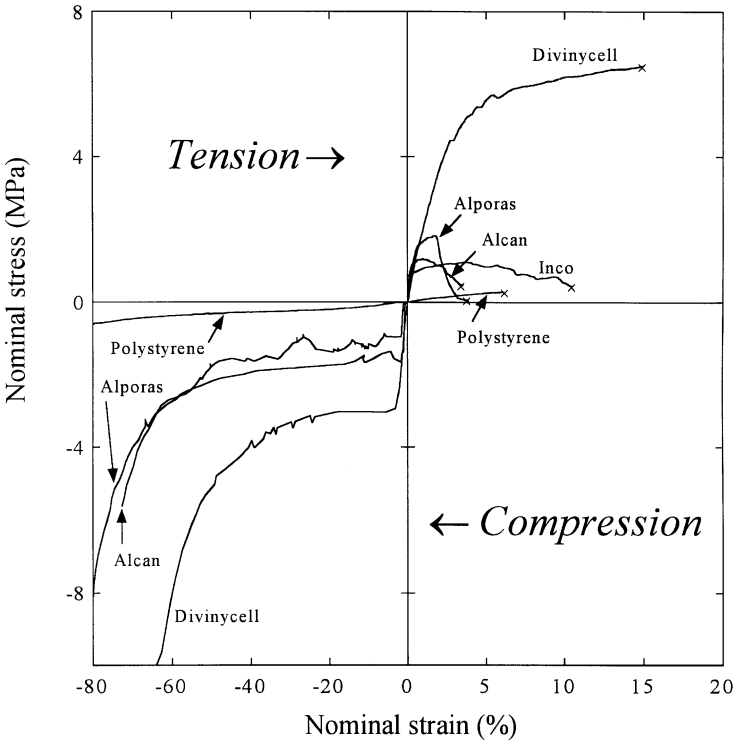

Fig. 1. Typical stress–strain curves for Alporas ($\bar{\rho} = 11\%$), Alcan ($\bar{\rho} = 5.7\%$), Inco ($\bar{\rho} = 4.2\%$), Divinycell ($\bar{\rho} = 14.3\%$) and Polystyrene ($\bar{\rho} = 3.0\%$) foams under uniaxial tension and compression.

W the specimen width, and B the thickness. The Inco foam was too thin to be tested in compression, and so only its tensile behaviour was measured.

Both unnotched and notched tests were performed at room temperature on a servo-hydraulic testing machine in displacement control at a rate of $0.02\,\text{mm}\,\text{s}^{-1}$ and $0.08\,\text{mm}\,\text{s}^{-1}$ for tensile and compressive loading, respectively. The load, grip displacement and the nominal axial strain (as measured by a clip gauge) were recorded. The measured nominal stress versus nominal strain curves for each of these foams under uniaxial tension and compression are shown in Fig. 1, for a nominal strain rate of $10^{-3}\,\text{s}^{-1}$.

Uniaxial tension and compression tests were then performed on foam panels containing a centre-hole of diameter D, as sketched in Fig. 2; the thickness B was the same as that used in the unnotched tests. For the specimens tested the width W lay in the range 10–500 mm and D/W was in the range 0–0.6. The ends of the specimens were reinforced with epoxy to avoid crushing by the grips, and the compressive loading platens were lubricated with PTFE spray to minimise friction.

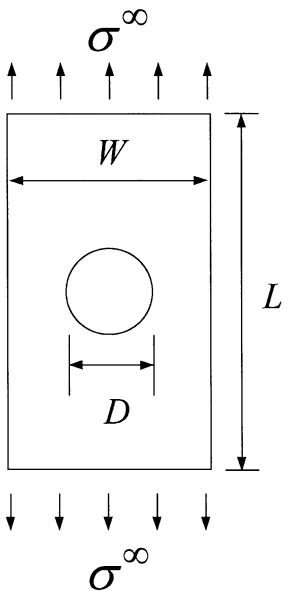

Fig. 2. Typical notched specimen with a centre-hole.

3. Effect of hole size upon measured tensile and compressive strengths

3.1. Tensile strength

Typical tensile and compressive stress–strain curves are shown in Fig. 2 for unnotched specimens of Alporas, Alcan, Inco, Divinycell and Polystyrene foams. Nominal stresses and strains are displayed throughout. The overall shapes of the stress–strain curves are similar for all foams considered. Additional details on the uniaxial stress–strain behaviours can be found in the references (Divinycell Technical Manual, 1995; Olurin et al. 2000; Kriszt and Ashby, 1997). The effect of the hole diameter D on the tensile net section strength is shown in Fig. 3 for Alporas, Alcan and Inco foams, and in Fig. 4 for Divinycell and Polystyrene foams. For the three metallic foams, no drop in tensile strength with increasing hole size is observed, to within material scatter. A small drop in net section strength is observed for the Divinycell foam, and a larger drop for the Polystyrene foam at a hole diameter D of about 10 mm, (see Fig. 4). There is some evidence that the net section strength for small hole diameters exceeds the ultimate tensile strength σ_{UTS}. The underlying explanation appears to be the heterogeneous nature of these materials. In unnotched tests, the specimens fail along the weakest plane, randomly located within the specimen. In a notched test, however, failure is at the net section, which may or may not coincide with the weakest microstructure of the specimen.

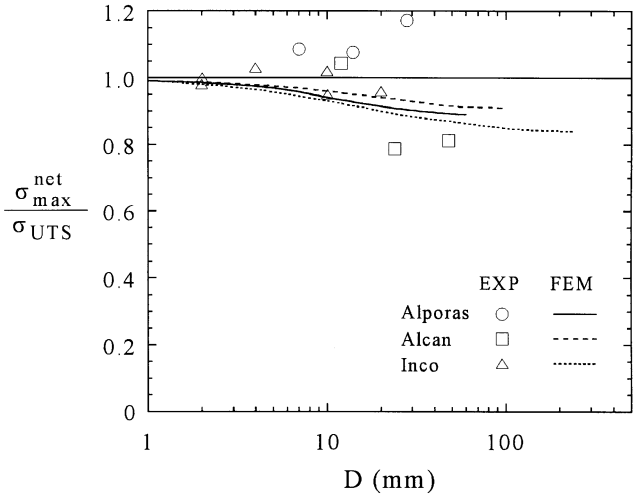

Fig. 3. Effect of hole diameter D upon the net section tensile strength σ^{net}_{max} of Alporas ($W = 70$ mm), Alcan ($W = 115$ mm) and Inco (geometrically similar specimen $D/W = 0.6$) foams.

The effect of hole diameter D normalised by the panel width W upon the *gross section strength* σ^{∞}_{max} is shown in Fig. 4(c) for the Divinycell foam. A clear trend emerges: with increasing width W of panel, the gross section strength reduces from the notch-insensitive strength to an intermediate value somewhat above the elastic–brittle line, as defined by

$$\sigma^{\infty}_{max} = \sigma_{UTS}(1 - D/W)/k_t, \tag{1}$$

where the net section elastic stress concentration factor k_t depends upon D/W. (Both the notch-insensitive and elastic–brittle strengths are displayed as bold lines in Fig. 4.) It is anticipated that tests on larger panels of Alporas and Alcan foams would reveal a similar switch in response from notch-insensitive to notch-sensitive; such tests were not possible in the current investigation due to limitations on the available size of materials and test machines.

3.2. Compressive strength

The gross section compressive strength is shown in Fig. 5 for the Alporas, Alcan, and Divinycell foams. Data are included for Alulight foam of composition Al–Mg1–Si0.6, as reported in McCullough et al. (1999). In all cases a notch-insensitive response was observed for all hole diameters investigated. This notch-insensitive behaviour is consistent with the ability of each foam to crush at a constant plateau stress σ_{pl}.

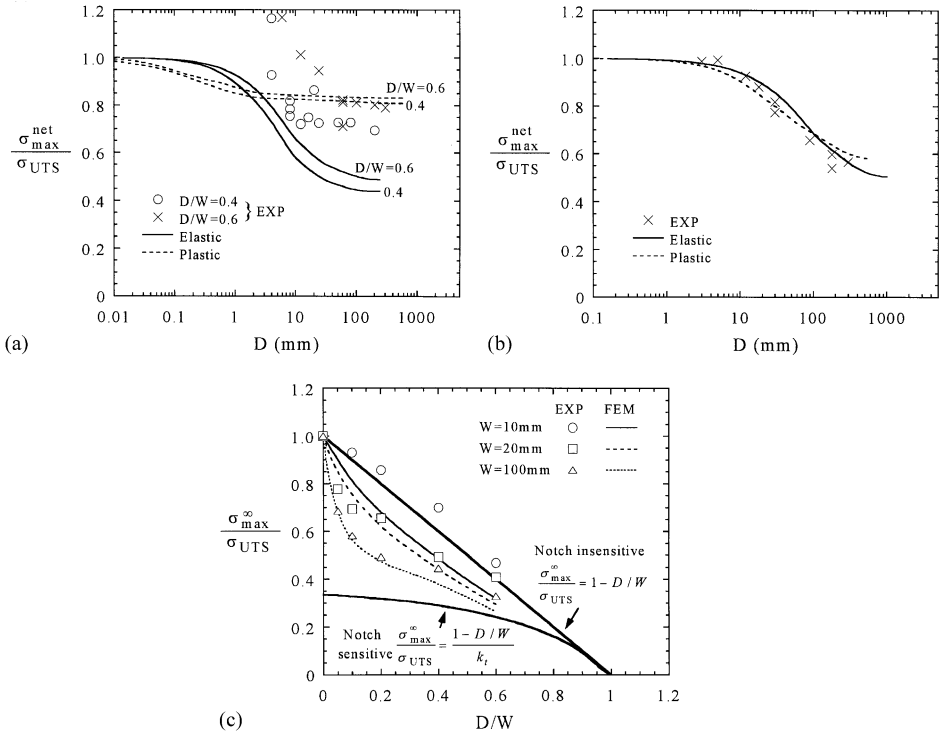

Fig. 4. Effect of the hole diameter on the tensile strength of foams with a centre-hole; (a) The net section strength versus the hole diameter D for Polystyrene foam, with $D/W = 0.60$; (b) The net section strength versus the hole diameter D for Divinycell PVC foam, with $D/W = 0.40$ and 0.60; (c) The gross section strength versus the specimen aspect ratio D/W for Divinycell PVC foam, with $W = 10$, 20, and 100 mm. The full and broken lines are the results of numerical model calculations described in the text.

4. A cohesive zone model for foams

A cohesive zone model of the tensile fracture of foams has been developed by Chen et al. (2000), in order to predict the notch-strength of foams for both pre-cracks and holes. The model assumes that the foam fails in a tensile mode and the failure mechanism in the foam is represented by a cohesive zone surrounded by an elastic–plastic compressible solid. The linear-softening traction versus crack opening law for the cohesive zone is characterised by the ultimate tensile strength σ_{UTS} and the critical stretch δ_0, see Fig. 6(a) and the foam is assumed to yield in accordance with the foam constitutive model proposed by Deshpande and Fleck (2000). (Observed crack traction versus opening behaviours for an open cell foam are detailed subsequently in Fig. 6b.)

There have been several attempts to develop constitutive models for ductile foams, mainly to capture the dependence of yielding of these materials upon hydrostatic pressure, with varying degrees of success (Gibson et al., 1989; Zhang et al., 1997;

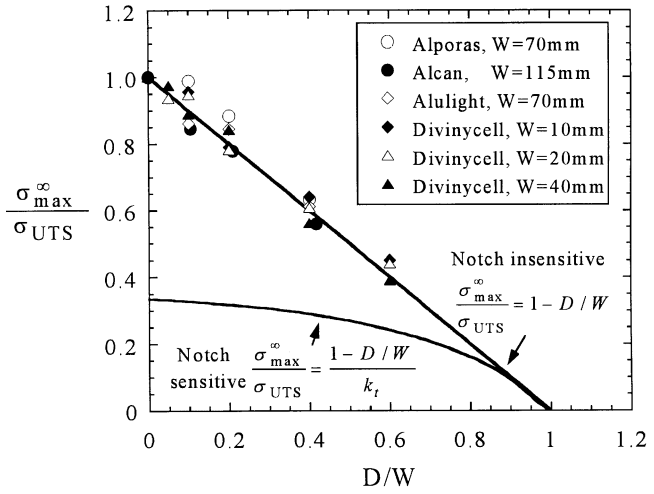

Fig. 5. Effect of the hole diameter on the compressive strength of foams with a centre-hole.

Miller, 2000). Recently, based on detailed multi-axial testing data, Deshpande and Fleck (2000, 2001) have developed a phenomenological constitutive model for both open and closed cell metallic and polymeric foams (of relative density less than 0.3) under proportional and nearly proportional loadings. Due to its simplicity, the self-similar yield surface model of Deshpande and Fleck (2000) is used in this paper, in conjunction with the method of finite elements, to characterise the constitutive behaviour of metallic and polymeric foams.

In the self-similar yield surface model, the yield function Φ is assumed to be

$$\Phi = \hat{\sigma} - Y = 0, \tag{2}$$

where Y is the uniaxial yield strength and $\hat{\sigma}$ is the effective stress, defined by

$$\hat{\sigma}^2 = \frac{1}{1+(\alpha/3)^2}(\sigma_e^2 + \alpha^2\sigma_m^2). \tag{3}$$

Here, α defines the aspect ratio of the elliptical yield surface in von Mises stress σ_e versus mean stress σ_m space. Note that for the case $\alpha = 0$, the effective stress $\hat{\sigma}$ reduces to σ_e and J_2-flow theory is recovered. Recent multi-axial yield experiments on metallic foams by Gioux et al. (2000) give additional support for the accuracy of Eq. (3).

For simplicity, isotropic hardening is assumed below, i.e. the yield surface grows in a geometrically self-similar manner with strain. This is supported by limited data on the yield surface of Alporas foams, as reported by Deshpande and Fleck (2000). To model the post-yield behaviour, an effective plastic strain rate $\dot{\hat{\varepsilon}}$, which is the work rate conjugate to $\hat{\sigma}$, is introduced as

$$\dot{\hat{\varepsilon}}^2 = [1+(\alpha/3)^2](\dot{\varepsilon}_e^2 + \dot{\varepsilon}_m^2/\alpha^2) \tag{4a}$$

in terms of

$$\dot{\varepsilon}_e^2 = (2/3)\dot{\varepsilon}_{ij}^p\dot{\varepsilon}_{ij}^p, \quad \text{and} \quad \dot{\varepsilon}_m = \dot{\varepsilon}_{ii}^p. \tag{4b}$$

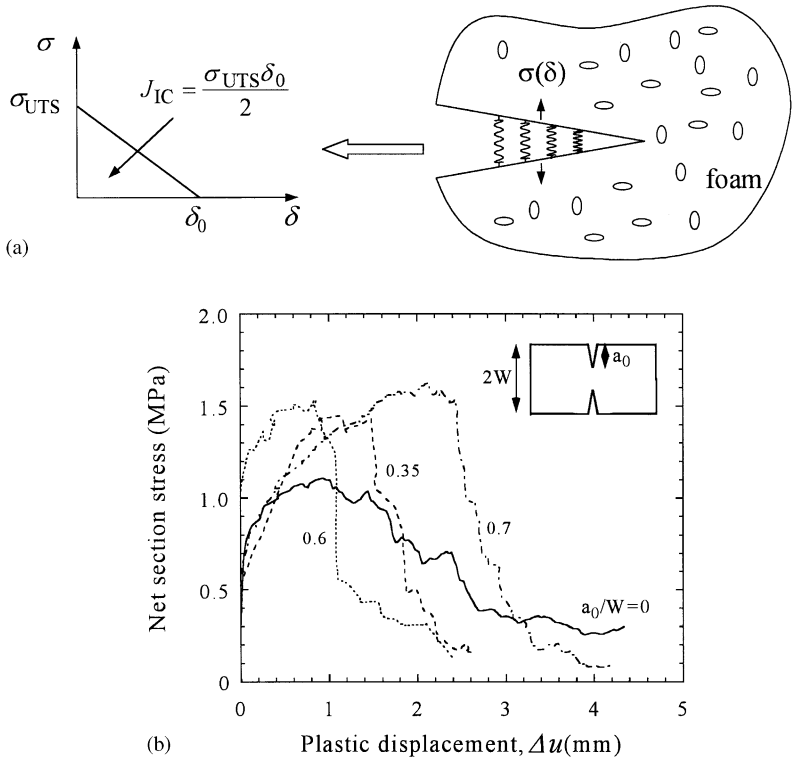

Fig. 6. (a) A sketch of the cohesive zone model with its bridging law; (b) Tensile net section stress versus plastic displacement Δu for Inco nickel foam ($\bar{\rho} = 4.2\%$, $2W = 15$ mm) with double edge notches. The ultimate tensile strength for the unnotched Inco foam σ_{UTS} equals 1.10 MPa.

Here, $\dot{\varepsilon}^{\mathrm{p}}_{ij}$ is the plastic strain rate, $i, j = 1$–3, and the summation convention over repeated indices applies. With the additional assumption of normality, the plastic strain-rate is given by

$$\dot{\varepsilon}^{\mathrm{p}}_{ij} = \dot{\hat{\varepsilon}} \frac{\partial \Phi}{\partial \sigma_{ij}}, \tag{5}$$

where the effective strain rate $\dot{\hat{\varepsilon}}$ is related to the effective stress rate by

$$\dot{\hat{\varepsilon}} = \frac{\dot{\hat{\sigma}}}{H(\hat{\sigma})}. \tag{6}$$

$H(\hat{\sigma})$ is the tangent of the uniaxial true stress versus logarithmic plastic strain curve at the stress level $\sigma = \hat{\sigma}$.

Except for the shape parameter α to be determined from experiment, the self-similar yield surface model by Deshpande and Fleck (2000) can be defined solely by a

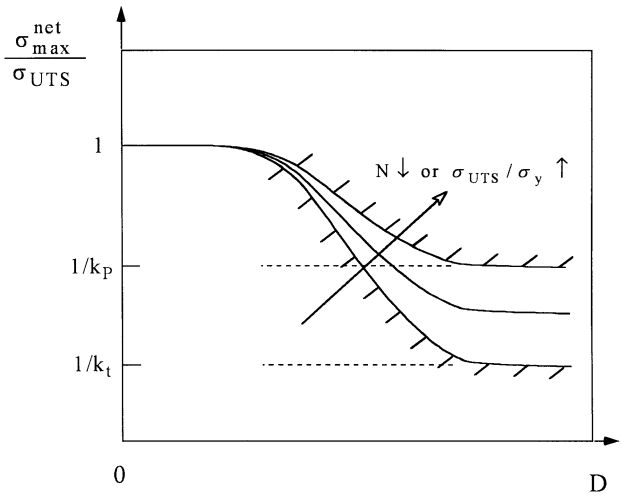

Fig. 7. A schematic drawing showing the ductile–brittle transition behaviour of the foams with a centre-hole.

uniaxial stress–strain curve which, in the present study, is assumed to have the form

$$\varepsilon = \begin{cases} \sigma/E, & \sigma \leqslant \sigma_y, \\ \varepsilon_y(\sigma/\sigma_y)^{1/N}, & \sigma > \sigma_y, \end{cases} \tag{7}$$

where E is the Young's modulus, σ_y and ε_y are the initial yield stress and strain, respectively, and N is the strain hardening exponent of the foam. The corresponding material parameters for each foam discussed in present study are given in Table 1.

The qualitative predictions of the cohesive zone model can be summarised as follows for the centre-hole specimen. At small hole diameters, the hole has only a minor influence upon the stress field across the net section, and the net section tensile strength σ_{max}^{net} is close to the ultimate tensile strength σ_{UTS}, as sketched in Fig. 7.

At larger D, the net section strength depends primarily upon the ratio of strength of bridging law, σ_{UTS}, to the yield strength of the solid, σ_y and upon the strain hardening exponent N. For the choice $\sigma_{UTS} \approx \sigma_y$ (or for large N), the cohesive zone fails with little attendant plasticity in the vicinity of the hole, and the panel fails in an elastic–brittle manner, with $\sigma_{max}^{net} = \sigma_{UTS}/k_t$. Alternatively, for $\sigma_{UTS} \gg \sigma_y$ (or small N), the structure undergoes plastic collapse before the cohesive zone fails, and the peak strength is set by the plastic stress concentration factor k_p for the hole, with $\sigma_{max}^{net} = \sigma_{UTS}/k_p$. For intermediate values of σ_{UTS}/σ_y, the centre-hole panel has a strength σ_{max}^{net} between σ_{UTS}/k_t and σ_{UTS}/k_p, see Fig. 7.

4.1. Material parameters for the cohesive zone model

The values of σ_{UTS} are given by the nominal tensile strengths, whereas the values of δ_0 listed in Table 1 are deduced by a range of methods, as follows. For the Inco

foam, the bridging law was measured directly by performing double deep notch tensile tests, with specimen geometry sketched in the insert of Fig. 6(b). Briefly, specimens of length 30 mm, thickness $B = 1.4$ mm and width $2W = 15$ mm were tested in uniaxial tension; a clip gauge of gauge length 8 mm was fastened along the centre line of the specimen, so that it straddled symmetrically the net section. Specimens of initial notch length $a/W = 0.35$–0.70 were loaded in tension, and the crack bridging law was taken as the net section stress versus plastic displacement from the clip gauge measurement. The results are plotted in Fig. 6(b), and, for each specimen, a value for δ_0 was deduced by equating the area under the traction versus extra displacement curve to $\sigma_{\mathrm{UTS}}\delta_0/2$. The overall average value of δ_0 was measured from tests with $a/W = 0.35$–0.70, and is reported in Table 1.

The critical bridging displacement δ_0 is related to J_{IC} by $\delta_0 = 2J_{\mathrm{IC}}/\sigma_{\mathrm{UTS}}$ since the traction–displacement law is triangular in shape, see Fig. 6. Thus, the value of δ_0 was deduced for the Alporas, Alcan, Alulight, Divinycell and Polystyrene foams from independent measurements of the initiation fracture toughness J_{IC}. The values of J_{IC} for Alporas and Alcan are taken from the experiments of Olurin et al. (2000) and for Alulight from the tests of McCullough et al. (1999); for these materials, compact tension specimens were employed and crack growth was measured visually and by electrical resistance methods. The polystyrene behaved in an elastic–brittle manner, and the J_{IC} value was deduced from the fracture load in double edge crack tests in tension: the average value of J_{IC} was taken from specimens of width = 30 mm, initial crack length = 4.5, 7.5 and 10.5 mm, and specimen thickness = 7 mm. The pre-crack was sharpened in each case using a razor blade.

The J_{IC} value of the Divinycell foam was determined by two different methods: (i) directly from a measured J_{R}–Δa crack growth resistance curve, and (ii) indirectly from the cohesive zone model and the measured steady state toughness J_{SS}. We consider each method in turn.

4.1.1. Method (i)

A crack growth resistance curve of J_{R} versus crack extension Δa was measured using a compact tension specimen of thickness $B = 10$ mm, width $W = 100$ mm and initial crack length $a_0 = 50$ mm. Crack advance was measured by an unloading compliance method, as detailed in the standard ASTM E399-90; the compliance measurements of crack extension were in good agreement with direct visual observations of the side-face of the specimen using a travelling microscope. The resulting curve is shown in Fig. 8; the initiation value J_{IC} of toughness was deduced from the intersection of the blunting line on a J versus Δa plot, and it was found that $J_{\mathrm{IC}} = 0.2\ \mathrm{kJm}^{-2}$. It is noted that J_{R} increases with crack extension from an initiation value J_{IC} to a steady state plateau value J_{SS}. A similar R-curve response has been reported for the metallic foams investigated in the study (Olurin et al. 2000), and the main origin of the R-curve has been traced to the development of bridging ligaments behind the crack tip. Now a word of caution. The J-blunting line procedure of the standard ASTM E399-90 was developed for small crack openings and for small offsets in crack growth in fully dense metals, and has no direct applicability to metallic foams. The measured value of J_{IC} is sensitive to the assumed offset in crack growth of the blunting line, and so

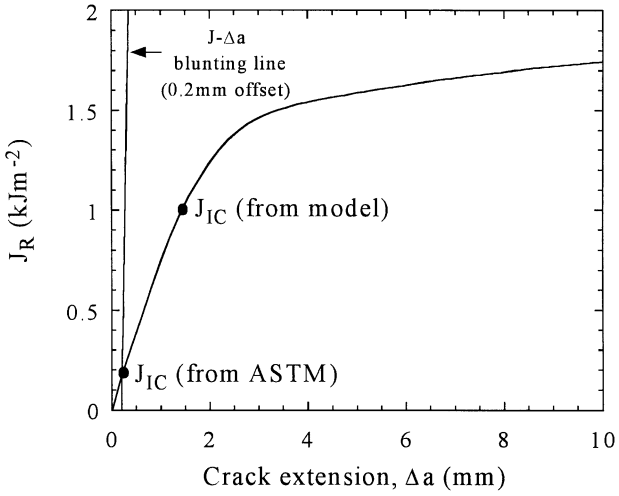

Fig. 8. Measured $J_R - \Delta a$ curve for Divinycell PVC foam ($\bar{\rho} = 14.3\%$) using compact tension specimen with $W = 100$ mm and $a_0 = 50$ mm.

we adopted the following rational method of deducing J_{IC} from the unambiguous J_{SS} value.

4.1.2. Method (ii)

The cohesive zone model was implemented in a boundary layer analysis of small scale yielding in order to predict the R-curve for the Divinycell foam. Full details of the method of analysis are reported elsewhere (Chen et al. 2000); the simulation was performed using measured values $(\sigma_y, \sigma_{UTS}, N, \alpha)$ for the elastic–plastic constitutive law (2)–(7) as listed in Table 1. The model gives a ratio of J_{SS}/J_{IC} equal to 1.6 independent of the assumed value of δ_0. On making use of the measured value $J_{SS} = 1.6\,\mathrm{kJ\,m^{-2}}$, we deduce that $J_{IC} = 1.0\,\mathrm{kJ\,m^{-2}}$; the critical opening $\delta_0 = 0.303$ mm follows immediately from the relation $\delta_0 = 2J_{IC}/\sigma_{UTS}$. It is noted that this value of J_{IC} exceeds the value obtained by method (i) by a factor of about 4, and we adopt this higher value of J_{IC} in subsequent analysis.

4.2. Numerical implementation

The cohesive zone model was implemented within the finite element program ABAQUS. To model crack growth, spring elements satisfying the linear softening bridging law of Fig. 6 are assigned on the net section of the centre-hole panel. The self-similar yield surface model, as summarised in Eqs. (2)–(7), was implemented via a user subroutine (Chen, 1998). Due to symmetry, only a quarter of each specimen is analysed, and discretised using about 10,000 four-node isoparametric elements in plane strain. Measured values of $(\sigma_y, \varepsilon_y, N, \alpha)$ and the Poisson ratio v are summarised in Table 1 for all foams considered in this study. Uniaxial tensile tests were used to determine all parameters, with α deduced from the measured plastic Poisson ratio.

5. Comparison of predictions with measured notch strength

The predictions of the cohesive zone model have been added to the plots of measured net section strength versus hole diameter D for Alporas, Alcan and Inco foams in Fig. 3 and for Divinycell and Polystyrene foams in Fig. 4. Consider first the predictions for the metallic foams. A mild notch sensitivity is predicted with increasing D: the net section strength drops by at most 20% as D is increased from 1 to 40 mm. The scatter in measured strength is of this order, and no size effect can be concluded unambiguously from the data. In contrast, the material scatter is reduced for the polymeric foams, and the observed strength drops by about 20% for Divinycell and by about 50% for Polystyrene, when D is increased from 1 to 100 mm, see Figs. 4(a) and (b), respectively. The cohesive zone model is in reasonable agreement with the measurements, given the material scatter at small hole sizes. For comparison, predictions are included in Figs. 4(a) and (b) for the linear-softening cohesive zone in an elastic solid, labelled as the elastic cohesive zone model. The effects of plasticity upon the predictions for Polystyrene is negligible due to the large measured value of $N = 0.71$: the uniaxial stress–strain curve is almost linear to fracture. The measurements confirm that the Polystyrene behaves in an elastic–brittle manner, with the tensile strength approaching $\sigma_{\mathrm{UTS}}/k_{\mathrm{t}}$ at large hole diameters. Divinycell behaves in a more plastic manner, and the elastic cohesive zone model underpredicts the notch strength at large D.

6. Concluding remarks

The compressive tests on centre-hole specimens reveal a notch-insensitive response for both metallic and polymeric foams: the net section strength equals the plateau strength of the unnotched foam.

In tension, the net section strength for centre-hole specimens shows a negligible size effect for metallic foams, a minor size effect for the plastic PVC foam Divinycell and a major size effect for the elastic–brittle foam Polystyrene. The large scatter in the observed strength of metallic foams is thought to be associated with the variability of strength at the net section. In particular, the notch strengthening apparent in Fig. 4 is, we believe, a consequence of the fact that the volume of highly stressed material in the vicinity of the hole is much less than that of an unnotched sample. Such statistical effects are not included in our analysis, although they are needed to explain the notch strengthening observed for small hole diameters in Fig. 4a. However, the observed transition in strength with increasing hole size cannot be explained simply by appealing to the usual statistical theories of strength such as that of Weibull: the observed strength displays a plateau at large hole diameters whereas statistical theories predict a continued drop in strength. In contrast, the elastic–plastic cohesive zone model appears to be successful in predicting the magnitude of the size effect in tension. The predicted drop in net section strength of the Polystyrene foam from σ_{UTS} to $\sigma_{\mathrm{UTS}}/k_{\mathrm{t}}$ is supported by observation, and may be explained in terms of a net section failure criterion at small D and a local maximum stress criterion at large D. For all other foams considered, the cohesive zone model suggests that the strength drops from σ_{UTS} to $\sigma_{\mathrm{UTS}}/k_{\mathrm{p}}$, as

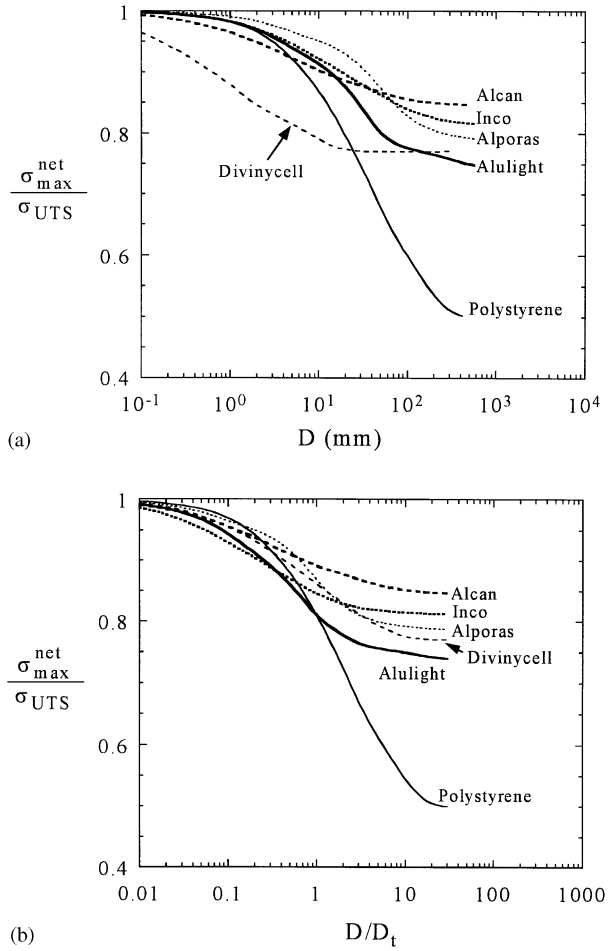

Fig. 9. Predicted ductile–brittle transition behaviour of foams with a central hole. (a) The tensile strength $\sigma^{net}_{max}/\sigma_{UTS}$ versus the hole diameter D; (b) The tensile strength $\sigma^{net}_{max}/\sigma_{UTS}$ versus the normalised hole diameter D/D_t.

follows. When the ultimate tensile strength σ_{UTS} of the foam is much greater than the yield strength σ_y, tensile failure at the edge of the hole occurs within a plastic zone, with the local peak stress set by the plastic stress concentration factor k_p; then, the net section tensile strength σ^{net}_{max} is given by σ_{UTS}/k_p.

The predicted hole size effect for the net section tensile strength of the metallic and polymeric foams is summarised Fig. 9; the predicted strength is plotted against the hole diameter D in Fig. 9(a). Data for the aluminium alloy foam Alulight is included, using the material parameters listed in Table 1. It is concluded from Fig. 9(a) that the four metallic foams considered all show a drop in net section strength by about 20% when D is increased from about 10 to 100 mm. A similar drop in strength is observed for the

plastic PVC foam Divinycell, with a transition hole size of about 1 mm. Polystyrene is the exception: it behaves in an elastic–brittle manner, and a predicted (and observed) drop in tensile strength by a factor of about 2 occurs at $D = 20$ mm.

It is instructive to normalise the net section strength $\sigma_{\max}^{\text{net}}$ by σ_{UTS}, and the diameter D by the transition value D_t, defined by

$$D_t \equiv \frac{EJ_{\text{IC}}}{\pi(1-\nu^2)\sigma_{\text{UTS}}^2}. \tag{8}$$

The resulting normalisation is shown in Fig. 9(b) and brings the predictions together, except for the large drop in strength for Polystyrene. The transition hole size D_t serves as a useful design parameter, as suggested by Chen et al. (2000): it is an approximate measure of the hole diameter at which the strength drops from the notch-insensitive limit to the notch-sensitive asymptote. Values of the transition hole diameter D_t are compared in Table 1 with the average cell size ℓ for each foam. It is clear that D_t is 1–2 orders of magnitude greater than ℓ.

Acknowledgements

The authors are grateful to DARPA/ONR for their financial support through MURI Grant Number N00014-1-96-1028 on the Ultra-light Metal Structures project under sub-contract to Harvard University, and to ONR contract N00014-9LJ-1916.

References

Ashby, M.A., Evans, A.G., Fleck, N.A., Gibson, L.J., Hutchinson, J.W., Wadley, H.N.G., 2000. Metal Foams: a Design Guide. Butterworth-Heinemann, Stoneham, MA.

Bao, G., Suo, Z., 1992. Remarks on crack-bridging concepts. Appl. Mech. Rev. 45, 355–366.

Chen, C., 1998. Manual for a UMAT user subroutine. Technical Report CUED/C-MICROMECH/TR.4, Engineering Department, Cambridge University.

Chen, C., Fleck, N.A., Lu, T.J., 2000. The mode I crack growth resistance of metallic foams. J. Mech. Phys. Solids 49(2), 231–259.

Cox, B.N., Marshall, D.B., 1994. Concepts for bridged cracks in fracture and fatigue. Acta Mater. 42, 341–363.

Deshpande, V.S., Fleck, N.A., 2000. Isotropic constitutive models for metallic foams. J. Mech. Phys. Solids 48, 1253–1283.

Deshpande, V.S., Fleck, N.A., 2001. Multiaxial yield behaviour of polymer foams. Acta Mater., in press.

Divinycell Technical Manual, 1995. Divinycell International AB, Box 201, S-312 22 LAHOLM, Sweden.

Evans, A.G., Hutchinson, J.W., Ashby, M.F., 1999. Multifunctionality of cellular metal systems. Prog. Mater. Sci. 43, 171–221.

Fleck, N.A., Kang, K.J., Ashby, M.F., 1994. The cyclic properties of engineering materials. Acta Mater. 42, 365–381.

Gibson, L.J., Ashby, M.F., 1997. Cellular Solids: Structure and Properties, 2nd Edition. Cambridge University Press, Cambridge.

Gibson, L.J., Ashby, M.F., Zhang, J., Triantafillou, T.C., 1989. Failure surfaces for cellular materials under multi-axial loads—I. Modelling. Int. J. Mech. Sci. 31, 635–663.

Gioux, G., McCormack, T.M., Gibson, L.J., 2000. Failure of aluminium foams under multi-axial loads. Int. J. Mech. Sci. 42, 1097–1117.

Kriszt, B.S., Ashby, M.F., 1997. Structure and properties of nickel foams. Technical Report, CUED/C-MATS/TR.240, Engineering Department, Cambridge University.

Lu, T.J., Stone, H.A., Ashby, M.F., 1998. Heat transfer in open cell metal foams. Acta Mater. 46, 3619–3639.

McCullough, K.Y.G., Fleck, N.A., Ashby, M.F., 1999. Toughness of aluminium alloy foams. Acta Mater. 47, 2331–2343.

Miller, R.E., 2000. A continuum plasticity model of the constitutive and indentation behaviour of foamed metals. Int. J. Mech. Sci. 42, 729–754.

Olurin, O.B., Fleck, N.A., Ashby, M.F., 2000. Deformation and fracture of aluminium foams. Mater. Sci. Eng. A291, 136–146.

Suo, Z., Ho, S., Gong, X., 1993. Notch ductile-to-brittle transition due to localised inelastic band. ASME J. Eng. Mater. Tech. 115, 319–326.

Zhang, J., Lin, Z., Wong, A., Kikuchi, N., Li, V.C., Yee, A.F., Nusholtz, G.S., 1997. Constitutive modelling and material characterisation of polymeric foams. ASME J. Eng. Mater. Tech. 119, 284–291.